Chapter 6

Quantum Dot in an External Magnetic Field

Since their first experimental realization [76] quantum dots have attracted a lot of attention from experimentalists and theorists alike. From the theoretical perspective they are ideal systems to study electron dynamics and correlation. A strong confinement in one direction makes the system quasi two-dimensional. In the remaining two spatial dimensions an electron feels a potential which is, in most cases, described by a parabolic potential [77, 78, 79, 80]. The effects of the host material can be taken into account using an effective mass m^*, dielectric constant ϵ^*, and gyromagnetic ratio g^*. The number of electrons in a quantum dot can be experimentally controlled ranging from one to around 1000 electrons. Therefore, quantum dots serve as an ideal laboratory for studying a large variety of many-body effects.

In this Chapter we apply the OEP equations in the collinear KLI approximation Eqs. (5.74)-(5.80) to a quantum dot in a constant external magnetic field $\mathbf{B}_0$. We first introduce the theoretical description of a quantum dot in Section 6.1 where we also simplify the collinear OEP-KLI equations using all symmetries of the considered system. We present the numerical results for 2 and 6 electron quantum dots in Sections 6.2 and 6.3, respectively. Although 2 and 6 electrons are both closed-shell systems for a parabolic quantum dot at zero magnetic field, the configurations quickly become open-shell when a magnetic field is applied.

6.1 Theoretical Description

Following Ferconi and Vignale [81], we describe a quantum dot as a system strictly confined to two dimensions (the x-y plane) with an external parabolic potential

$$v_0 = \frac{1}{2}\omega^2 r^2, \qquad r^2 = x^2 + y^2. \tag{6.1}$$

The external magnetic field B_0 is constant along the z-direction

$$\mathbf{B}_0(\mathbf{r}) = B_0\, \mathbf{e}_z, \tag{6.2}$$

i.e. perpendicular to the quantum dot. The corresponding external vector potential is then (in symmetric gauge) given by

$$\mathbf{A}_0(\mathbf{r}) = \frac{B_0}{2}\, r\, \mathbf{e}_\theta, \tag{6.3}$$

where $\mathbf{e}_\theta$ denotes the angular direction in the plane. The whole problem is therefore cylindrically symmetric.

Since we apply the collinear approximation, we use the spin-dependent scalar exchange-correlation potentials and the vector potential as basic variables. Under the assumption that the exchange-correlation potentials preserve the cylindrical symmetry of the problem, i.e.

$$\begin{aligned} v_{xc\sigma}(\mathbf{r}) &= v_{xc\sigma}(r), & (6.4)\\ \mathbf{A}_{xc}(\mathbf{r}) &= A_{xc}(r)\mathbf{e}_\theta & (6.5) \end{aligned}$$

the KS Hamiltonian (in symmetric gauge) is given by

$$\begin{aligned} \hat{H}^{KS}_\sigma &= -\frac{1}{2}\left[\frac{\partial^2}{\partial r^2} + \frac{1}{r}\frac{\partial}{\partial r} + \frac{1}{r^2}\frac{\partial^2}{\partial\theta^2}\right] - \frac{i}{2c}B_0\frac{\partial}{\partial\theta} + \frac{1}{2}\omega_0^2\, r^2 + \frac{1}{2c^2}\frac{B_0^2}{4}r^2 \\ &\quad + g\,\mu_B\, s_\sigma\, B_0 + v_H(r) + v_{xc\sigma}(r) - \frac{i}{c}\frac{A_{xc}(r)}{r}\frac{\partial}{\partial\theta}, \end{aligned} \tag{6.6}$$

where $s_\sigma = \pm 1/2$ depending on the spin of the particle. Due to the cylindrical symmetry of the problem we can use the product ansatz

$$\varphi_{jl\sigma}(\mathbf{r}) = \exp(i\, l\, \theta) R_{jl\sigma}(r) \tag{6.7}$$

for the KS orbitals. Applying the KS Hamiltonian (6.6) to this wave function we obtain the eigenvalue equation for the radial part $R_{jl\sigma}(r)$

$$\begin{aligned} \Bigg[-\frac{1}{2}\left(\frac{\partial^2}{\partial r^2} + \frac{1}{r}\frac{\partial}{\partial r} - \frac{l^2}{r^2}\right) + \frac{l}{2}\,\omega_c + \frac{\Omega^2}{2}r^2 + g\,\mu_B\, s_\sigma\, B_0 \\ - \frac{l}{c}\frac{A_{xc}(r)}{r} + v_H(r) + v_{xc\sigma}(r)\Bigg] R_{jl\sigma}(r) = \epsilon_{jl\sigma} R_{jl\sigma}(r) \end{aligned} \tag{6.8}$$

with the cyclotron frequency $\omega_c = B_0/c$ and $\Omega = \sqrt{\omega_0^2 + \omega_c^2/4}$.

For non-interacting particles, where $v_{xc\sigma} = v_H = A_{xc} = 0$, the eigenvalue problem reduces to a harmonic oscillator with frequency Ω and eigenvalues shifted by $\omega_c l/2 + g\mu_B s_\sigma B_0$ and can be solved analytically. The resulting eigenfunctions

$$f_{jl}(r) = \frac{\sqrt{2}}{a_0}\sqrt{\frac{j!}{(j+\mid l\mid)!}}\left(\frac{r}{a_0}\right)^{|l|}\exp\left(-\frac{r^2}{2a_0^2}\right) L_j^{|l|}\left(\frac{r^2}{a_0^2}\right), \tag{6.9}$$

where $a_0 = \sqrt{1/\Omega}$ and $L_j^{|l|}$ denote the associated Laguerre polynomials, are used as basis functions for expanding the radial part of the Kohn-Sham orbitals. The eigenvalues $\varepsilon_{jl\sigma}$ of the non-interacting problem read

$$\varepsilon_{jl\sigma} = \Omega\,(2j+ \mid l \mid +1) + \frac{B_0}{2}\left(\frac{l}{c} + 2g\;\mu_B\;s_z\right). \tag{6.10}$$

Using the cylindrical symmetry the numerical implementation only concerns the radial part and is therefore one-dimensional. All radial functions, KS orbitals as well as all potentials, are treated on an equally spaced grid. Expanding in the basis set (6.9) the KS eigenvalue equation reduces to a matrix equation for the expansion coefficients which can be solved using standard linear algebra libraries. Convergence tests show that the inclusion of 10 basis functions for each angular momentum is absolutely sufficient.

The spin densities of the system (5.35) are given by

$$n_\sigma(r) = \sum_{jl}^{N_\sigma} R_{jl\sigma}^2(r) \tag{6.11}$$

and the paramagnetic current density has only a non-vanishing θ-component

$$j_p(r) = \sum_{\sigma=\uparrow,\downarrow}\sum_{jl}^{N_\sigma} \frac{l}{r}\,R_{jl\sigma}^2(r). \tag{6.12}$$

Although this term seems to diverge at $r = 0$ it is well defined. Actually, it is equal to zero at the origin for all l because of the factor $r^{|l|}$ in $R_{jl\sigma}$. The 3×3 matrix $\mathcal{N}$ (5.77) reduces to a scalar quantity given by

$$\mathcal{N}(r) = \sum_{\sigma=\uparrow,\downarrow}\sum_{jl}^{N_\sigma} \frac{l^2}{r^2} R_{jl\sigma}^2(r) \tag{6.13}$$

approaching a finite value for $r \to 0$. Hence, the cylindrical symmetry causes a further simplification of the OEP-KLI equation (5.74) to a 3×3 matrix equation again denoted as

$$\mathcal{D}(r)\mathcal{V}_{xc}(r) = \mathcal{R}(r), \tag{6.14}$$

where the potential vector is now given by

$$\mathcal{V}_{xc}(r) = \left((v_{xc\uparrow}(r), v_{xc\downarrow}(r), \frac{1}{c}A_{xc}(r)\right). \tag{6.15}$$

The matrix $\mathcal{D}$ reads

$$\mathcal{D} = \begin{pmatrix} n_\uparrow(r) & 0 & j_{p\uparrow}(r) \\ 0 & n_\downarrow(r) & j_{p\downarrow}(r) \\ j_{p\uparrow}(r) & j_{p\downarrow}(r) & \mathcal{N}(r) \end{pmatrix}, \tag{6.16}$$

where $j_{p\sigma}$ denote the spin-components of (6.12). The first two components of $\mathcal{R}$ on the rhs of Eq. (6.14) are still given by

$$\mathcal{R}_1(r) = \frac{1}{2}\sum_{k=1}^{N_\uparrow}\left(\varphi^*_{k\uparrow}(\mathbf{r})\frac{\delta E_{xc}^{\mathrm{EXX}}}{\delta\varphi^*_{k\uparrow}(\mathbf{r})} + n_{k\uparrow}(\mathbf{r})D^*_{kk\uparrow} + c.c.\right), \tag{6.17}$$

$$\mathcal{R}_2(r) = \frac{1}{2}\sum_{k=1}^{N_\downarrow}\left(\varphi^*_{k\downarrow}(\mathbf{r})\frac{\delta E_{xc}^{\mathrm{EXX}}}{\delta\varphi^*_{k\downarrow}(\mathbf{r})} + n_{k\downarrow}(\mathbf{r})D^*_{kk\downarrow} + c.c.\right), \tag{6.18}$$

where we have chosen the exact-exchange functional E_{xc}^{EXX} given in Eq. (5.82) as the specific approximation for E_{xc} to be used in the numerical implementation. However, the form of D from (5.76) simplifies to

$$D^*_{kj\sigma} = \int d^2r' \left(v_{xc\sigma}(\mathbf{r}')\varphi_{k\sigma}(\mathbf{r}')\varphi^*_{j\sigma}(\mathbf{r}') - \varphi^*_{j\sigma}(\mathbf{r}')\frac{\delta E_{xc}^{\mathrm{EXX}}}{\delta\varphi^*_{k\sigma}(\mathbf{r}')}\right. \tag{6.19}$$

$$\left. -\frac{i}{2c}A_{xc}(\mathbf{r}')\left[\varphi^*_{j\sigma}(\mathbf{r}')\frac{\partial\varphi_{k\sigma}(\mathbf{r}')}{\partial\theta'} - \varphi_{k\sigma}(\mathbf{r}')\frac{\partial\varphi^*_{j\sigma}(\mathbf{r}')}{\partial\theta'}\right]\right), \tag{6.20}$$

where we suppressed the indices for angular momenta in both $\mathcal{R}$ and D. The third component of $\mathcal{R}$ is given by

$$\mathcal{R}_3(r) = \frac{1}{2}\sum_{\sigma=\uparrow,\downarrow}\sum_{k=1}^{N\sigma}\left(\frac{1}{2i}\varphi^*_{k\sigma}(\mathbf{r})\frac{\partial}{\partial\theta}\frac{\delta E_{xc}^{\mathrm{EXX}}}{\delta\varphi^*_{k\sigma}(\mathbf{r})} - \frac{1}{2i}\frac{\partial\varphi^*_{k\sigma}(\mathbf{r})}{\partial\theta}\frac{\delta E_{xc}^{\mathrm{EXX}}}{\delta\varphi^*_{k\sigma}(\mathbf{r})}\right.$$

$$\left. + j_{pk\sigma}(r)D^*_{kk\sigma} + c.c.\right). \tag{6.21}$$

Although it may look as if the components of $\mathcal{R}$ acquire some dependence on θ, all these contributions cancel due to the special form of the wave function (6.7).

6.2 Results for 2 electrons

As a first application we consider a 2-electron quantum dot. All calculations are performed for GaAs quantum dots. GaAs is described by an effective mass $m^* = 0.067$, a dielectric constant $\epsilon^* = 12.4$, and a gyromagnetic ratio $g^* = -0.44$. For 2 electrons there are only two possible spin configurations, either the two spins are parallel or anti-parallel. At zero magnetic field, the anti-parallel configuration is the ground-state. Both electrons occupy the $l = 0$ orbital and $j_p = 0$. As a result the exchange vector potential vanishes identically and the calculation reduces to the spin-DFT case. Increasing the external magnetic field beyond 0.84 T (we use $\omega_0 = 5$ meV as external confinement) the parallel configuration becomes energetically favoured. Then, due to the Pauli-exclusion principle, one of the electrons has to occupy the $l = -1$ state, see Eq. (6.10). Hence, the ground-state carries a current

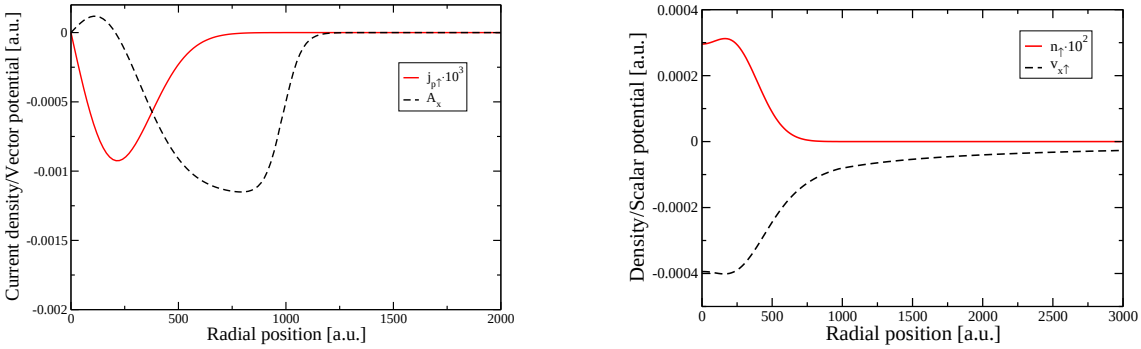

Figure 6.1: The paramagnetic current density and the exchange vector potential (left) and the density and the scalar potential (right) for 2 electrons in a quantum dot with $\omega_0 = 5$ meV and an applied magnetic field of 1 T.

and the calculation yields a non-zero exchange vector potential as shown in Fig. 6.1 for an external magnetic field of 1 Tesla. The non-vanishing density at the origin is due to the occupied $l = 0$ state. In addition the density has a maximum at around 250 a.u. due to the $l = -1$ state, see Fig. 6.1.

As one can see in Fig. 6.1, the grid was chosen large enough to reach the asymptotic $-1/r$ region of the scalar exchange potential. The density and also the current density are negligible beyond 700 a.u. As a result the 3×3 matrix (6.16) becomes singular and Eq. (6.14) cannot be inverted to determine $v_{x\sigma}$ and A_x. While the asymptotic form of the scalar potential is known and explicitly set to $-1/r$ the asymptotic behavior of the vector potential is so far unknown. Its determination is rather involved because the leading order in r in the OEP-KLI equations is always determined by the scalar potential. From this leading order, we only know that the vector potential has to converge to zero. Therefore, in the numerical implementation, we set the scalar potentials to $-1/r$ asymptotically and obtained the vector potential from the third component of $\mathcal{D}(r)\mathcal{V}_x(r)$ by adding a small constant to $\mathcal{N}$ to avoid the singularity. As a consequence, the form of the vector potential beyond 700 a.u. in Fig. 6.1 is artificial. However, the specific form of the vector potential does not influence the results for the total energy because there it is multiplied by the current density which is practically zero in that region.

For the parallel spin configuration the application of an external magnetic field has exactly the same effect as changing the external confinement. Hence, LDA calculations for different confinements ω_0 at zero external magnetic field have been employed to mimic the effects of an external magnetic field [78]. The same calculation in CSDFT using the exact-exchange functional yields the results for the scalar and the vector exchange potentials shown in Fig. 6.2. The shapes compare very well with those in Ref. [78]. However, in this reference the plots are given in arbitrary units which makes a quantitative comparison impossible. The scalar and the vector exchange potential show the expected trends for different confinements. For larger

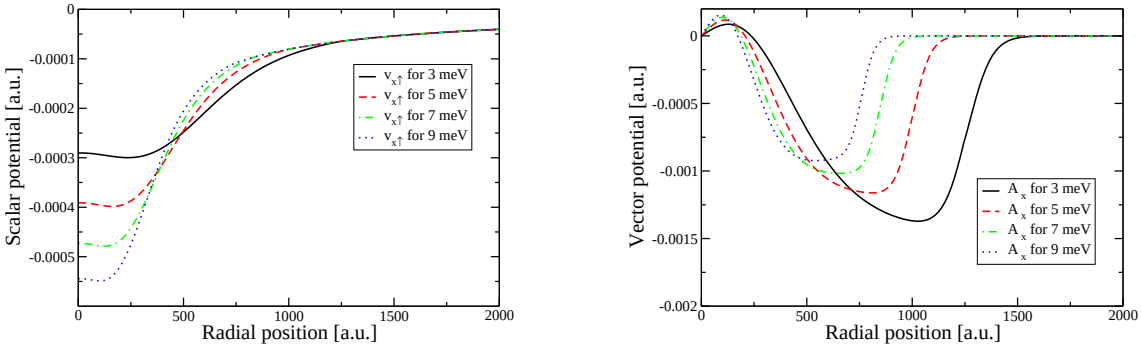

Figure 6.2: The scalar exchange potential (left) and the exchange vector potential (right) for 2-electron quantum dots with different confinement ω_0 at zero magnetic field.

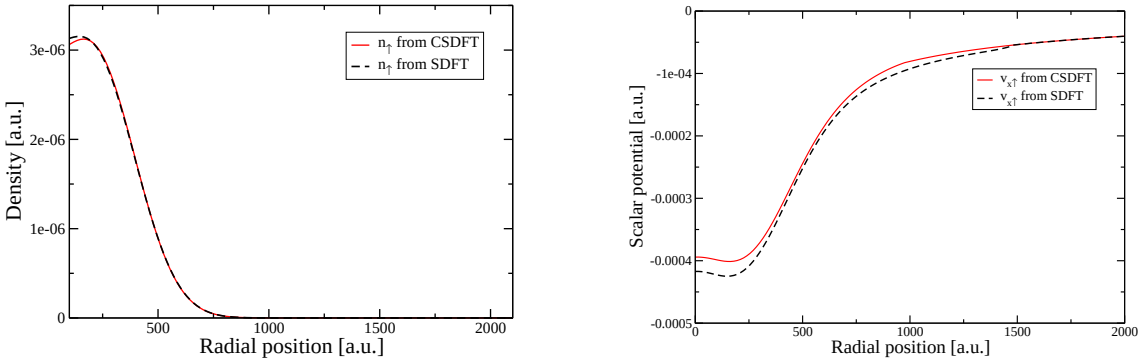

Figure 6.3: The density (left) and the scalar exchange potential (right) for 2-electron quantum dots with $\omega_0 = 5$ meV at $B_0 = 1$ T from CSDFT and SDFT calculations. The SDFT calculation contains the coupling to A_0.

confinement the asymptotic region starts at smaller radial positions. Consequently, the potentials become stronger around the origin as the confinement increases.

It is also interesting to compare a CSDFT with a corresponding SDFT calculation. The differences in the calculated densities and scalar exchange potentials, shown in Fig. 6.3, are very small. However, one should note that the SDFT calculation contains the coupling to the external vector potential A_0. This is kind of artificial since any DFT calculation containing an additional external potential should also contain the corresponding exchange-correlation potential. Neglecting the coupling of orbital angular momenta to A_0 leads to very different results in the SDFT calculation. Due to the small difference in the scalar potentials and the densities and the small size of the exchange vector potential the total energies in CSDFT and SDFT hardly differ. For our 2 electron quantum dot the total energy in CSDFT is $6.843 \cdot 10^{-4}$ Ha while the SDFT calculation yields $6.844 \cdot 10^{-4}$ Ha. The

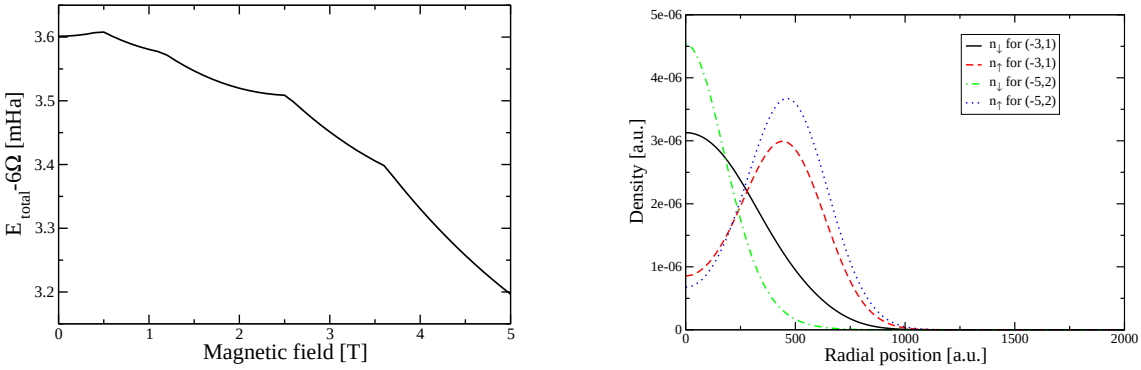

Figure 6.4: The energy $E_{\text{total}} - 6\Omega$ of the ground-state as a function of external magnetic field (left) and the densities at 1.2 T for two different configurations. The quantum dot contains 6 electrons and the confining strength is 5 meV.

total energy of the CSDFT calculation is lower than the energy in SDFT due to the additional variational freedom provided by the exchange vector potential. However, the difference in the energies is of the order of the theoretical error from forcing the vector potential asymptotically to zero without knowing the correct asymptotic behavior.

6.3 Results for 6 electrons

Here, we consider 6 electrons forming the next closed-shell system for a 2D parabolic quantum dot beyond the 2 electron case discussed before. The states (L_z, S_z) are usually denoted by their total angular momentum L_z and their total spin S_z. At zero magnetic field, in the ground-state, the $l = 0$ and the $l = \pm 1$ orbitals are occupied with 2 electrons each, i.e. the ground-state is (0,0). Increasing the magnetic field, different configurations become energetically more favoured. For a parabolic confinement of 5 meV the spin-down electron in the $l = +1$ state is flipped and occupies the $l = -2$ state at around 0.5 T. The configuration is hence changed to (-3,1). Increasing the magnetic field further the spin-down electron in the $l = -1$ state flips its spin and its angular momentum becomes $l = -3$ at a magnetic field of about 1.2 T resulting in (-5,2). At 2.6 T the remaining spin-up electron in the $l = +1$ orbital is transferred to the $l = -4$ state, (-10,2), before the system becomes completely spin polarized at 3.6 T occupying $l = 0$ to $l = -5$ states leading to the configuration (-15,3). The energy of the system with increasing magnetic field is shown in Fig. 6.4. The transitions

$$(0, 0) \rightarrow (-3, 1) \rightarrow (-5, 2) \rightarrow (-10, 2) \rightarrow (-15, 3) \tag{6.22}$$

lead to the kinks in the energy, while a given state has a parabolic dependence on the external magnetic field. Subtraction of 6Ω corrects for the energy gain due to

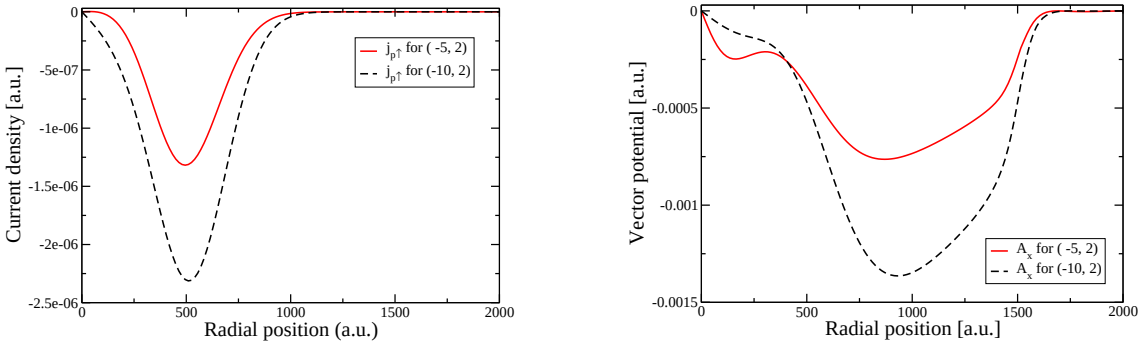

Figure 6.5: The paramagnetic current densities for two different configurations at 2.0 T (left) and the corresponding exchange vector potentials (right). The quantum dot contains 6 electrons and the confining strength is 5 meV.

the increasing confinement. Whenever a new configuration is occupied all densities change discontinuously. In Fig. 6.4 we plot the densities of the (-3,1) and the (-5,2) configurations at 1.2 T, where the ground-state configuration changes from the former to the latter. The spin-up density increases as expected while the spin-down density is reduced. The changes are quite dramatic while the energy of course changes continuously over the whole range from 0 to 5 T. We emphasize that there is no interpolation between different functionals at high and low magnetic fields in our calculation. One and the same functional is employed for all external magnetic fields.

Due to the increased angular momenta compared to the 2 electron system, the current density shows more structure.The larger the angular momentum the more enhanced is the current density, see Fig. 6.5. Also, the maximum is slightly shifted to larger radial position, as expected. The corresponding vector potentials are also shown in Fig. 6.5. Again, the configuration with larger angular momentum yields a larger exchange vector potential. The minimum close to the origin for the (-5,2) configuration vanishes and the second minimum is significantly enhanced. Therefore, the first minimum must be due to the $l = +1$ state which is no longer occupied in the (-10,2) configuration. The spin is the same in both configurations and therefore cannot influence the vector potential.

A comparison of CSDFT and SDFT again reveals very little difference in the densities and scalar exchange fields. Also the total energies only differ on the order of the error introduced by the unknown asymptotics of A_x. Again, it should be noted that the SDFT calculation contains the coupling to the external vector potential. In other words, we have to conclude that taking or not taking the exchange vector potential into account makes very little difference, at least for the systems studied so far.